PHYSICAL REVIEW E **94**, 053208 (2016)

Finite-temperature quantum effects on confined charges

Jeffrey Wrighton and James Dufty
Department of Physics, University of Florida, Gainesville, Florida 32611, USA

Sandipan Dutta
Center for Soft and Living Matter, Department of Physics, Ulsan National Institute of Science and Technology, Ulsan 689-798, Republic of Korea

(Received 1 June 2016; published 21 November 2016)

A quantum system of N Coulomb charges confined within a harmonic trap is considered over a wide range of densities and temperatures. A recently described construction of an equivalent classical system is applied in order to exploit the rather complete classical description of harmonic confinement via liquid-state theory. Here, the effects of quantum mechanics on that representation are described with attention focused on the origin and nature of shell structure. The analysis extends from the classical strong Coulomb coupling conditions of dusty plasmas to the opposite limit of low temperatures and large densities characteristic of "warm, dense matter."

DOI: 10.1103/PhysRevE.94.053208

I. INTRODUCTION AND MOTIVATION

Coulomb correlations have been the focus of intense study for more than 50 years. Weak-coupling conditions, both classical and quantum, are now well understood. The more interesting and difficult conditions of strong Coulomb coupling are well understood only in the limiting cases of zero temperature (electrons) and high temperatures (classical ions). Renewed interest in the intermediate crossover domain between quantum and classical limits at arbitrary coupling has followed from new experimental studies of "warm, dense matter" [1], new theoretical approaches [2–6], and new path-integral Monte Carlo simulations [7]. The objective here is to explore this domain of finite temperatures for the case of charges in a harmonic trap under conditions where confinement, strong coupling, and quantum effects can appear together. Of particular interest is the role of these conditions in the formation and characterization of shell structure. The classical origins of shell structure are now well understood via theory, simulation, and experiment [8–17]. The focus here is on exploring modifications of these mechanisms due to quantum effects. No attempt is made in this initial study to provide a detailed model for the wide class of related experimental conditions of nanophysics [18–21] or ultracold gases [22,23]. Such models are planned to evolve from the results presented here.

The approach here is to exploit classical many-body methods that treat Coulomb coupling effectively, such as classical density functional theory [24], liquid-state theory [25], or molecular dynamics simulation [26]. It is necessary first to embed relevant quantum effects in a classical statistical mechanics. This has been shown to be an accurate and practical idea recently by Perrot and Dharma-wardana [2] using liquid-state theory by introducing a pair potential modified to include exchange and diffraction effects and an effective temperature to admit a finite kinetic energy at zero temperature. This approach was formalized for a more precise context by two of the current authors [3], and a preliminary application to confined charges was described [4]. This effective liquid-state approach has proved accurate for the thermodynamics and structure of the three-dimensional uniform electron gas over a wide range of densities and temperatures [5,6] in comparison to recent path-integral Monte Carlo simulations [7]. Dharma-wardana and Perrot have applied this approach broadly to the two-dimensional electron gas and electron layers to study the exchange-correlation energies, distribution functions, and the spin-polarized phases [27–29]. More recently, Dharma-wardana has applied his classical map to calculating properties for warm, dense matter via a classical density functional theory. Reviews of this latter work are given by Refs. [30–32]. The classical map method, although not broadly adopted, is a rare theoretical approach that can be applied broadly across the temperature-density plane and has demonstrated significant success to date.

The above applications are to uniform thermodynamic states, while here a strongly nonuniform system is considered. This approach is particularly useful for the problem posed here since there is now a rather complete study of the classical "Coulomb balls" via liquid-state theory and classical Monte Carlo simulations [16,17]. Hence, the classical theory can be adopted directly, once the effective quantum potentials and thermodynamic parameters are specified, to address the questions of quantum effects on shell formation driven by classical Coulomb strong coupling. That is the objective of the work presented here.

At equilibrium the harmonically confined system is specified by the average number of particles in the trap, $\overline{N}$, the temperature, T, and the strength of the confining potential. The latter determines the volume of the system (see below) so that ultimately the harmonic potential parameters can be expressed in terms of the density and temperature. In the classical limit, all density and temperature dependence of dimensionless quantities occurs only through the classical Coulomb coupling constant, $\Gamma \equiv q^2/(r_0 k_B T)$, where q is the charge and r_0 is the Wigner-Seitz length related to the average global density $\overline{n}$ by $r_0 = (4\pi\overline{n}/3)^{-1/3}$. It is a measure of the Coulomb energy for a single pair of charges relative to the average kinetic energy per particle, $q^2/k_B T r = \Gamma/r^*$, where $r^* = r/r_0$. In the classical case the primary results are that shell structure (peaks in the radial density profile) appear at sufficiently strong coupling ($\Gamma \gtrsim 10$) and sharpen as the coupling increases. The number of shells is determined entirely by $\overline{N}$. A mean-field description, without correlations, yields no shell structure at any value of Γ. The equivalent classical

system with quantum effects has a modified behavior. Here, these quantum effects are studied for the case of $\Gamma = 20$, where the classical mechanism for shell formation is active. Hence, the focus is on modification of the classical shell structure as well as possible new formation of shells. A wide range of temperatures and densities are studied, all corresponding to $\Gamma = 20$, from weak to very strong quantum effects. Initial study of a simple model [4] showed the emergence of a new origin for shell structure even at weaker coupling due to exchange effects (Fermi statistics) on the shape of the confining potential. That simple model is reconsidered here in Sec. III. However, an improved model considered in Sec. IV shows that mechanism to be significantly diminished [33]. The objective here is to explore the onset and competition for all of the potential origins for shell structure—Coulomb correlations, diffraction, exchange—as a function of the dimensionless density parameters $r_s = r_0/a_b$ (where a_b is the Bohr radius in terms of the charge and mass of the confined particles) and $t = k_B T/e_F$ (where e_F is the ideal gas Fermi energy per particle, again in terms of the confined particle's mass).

To explore the full range of systems of interest requires a wide range of values for t and r_s. The upper limits are primarily imposed by the conditions of strong coupling for classical shell structure, as occurs in dusty plasmas. This is illustrated in Fig. 1. For $r_s < 10$ Coulomb effects are weaker and the classical-quantum transition is dominated by t, for ideal gas diffraction and exchange effects. Here the classical domain has been defined as $t > 10$. In contrast, for larger r_s quantum effects on Coulomb correlations dominate at higher t and the coupling strength Γ is changed to an effective value $\Gamma_e(t,r_s) \leqslant \Gamma$ [see Eq. (15) below]. The classical limit in this domain is defined to be $\Gamma_e/\Gamma > 0.99$. Typical experimentally accessible values for electrons are $r_s < 10$ over a wide range of temperatures. This is the domain of zero-temperature condensed-matter physics, warm dense matter, and Debye plasmas in the left side of Fig. 1. At the opposite extreme are the strongly coupled classical plasmas in the upper right side of the figure. These large values of t and r_s can be realized only for particles of large mass and charge, e.g., dusty plasmas [34,35]. Intermediate domains are the primary interest here. The constant Γ lines are shown for $\Gamma = 1$ and 20. The crosses on these lines indicate values of t,r_s for which calculations are reported here. Since the parameter space is large only the case $\overline{N} = 100$ is considered, to focus only on quantum effects on the density profile for conditions where shell structure is already present in the classical limit. Smaller values of Γ and $\overline{N}$ would have weaker and fewer shells, respectively. Also, only the fluid phase for unpolarized charges is considered; for the crystal phase or other polarization phases, see Refs. [27–29,36].

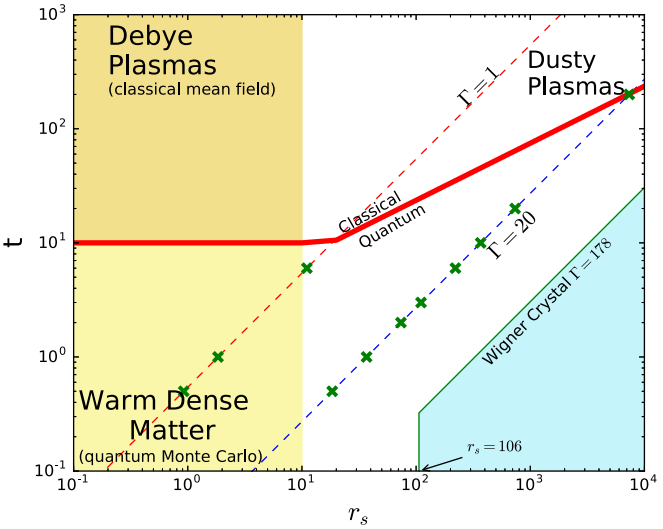

FIG. 1. Values of r_s and t of interest. Note that the values correspond to a range of experimental conditions from electrons to dusty plasmas. A definition of the crossover to quantum effects from classical behavior is shown. Crosses indicate the conditions studied in Secs. III and IV.

The next section defines the effective classical description for the density profile of the quantum system in terms of the modified pair potential and confining potential; all quantum effects occur through modifications of the underlying Coulomb and harmonic forms, respectively. The approximate form for the pair potential is described in Appendix A. As noted above, it has been shown to give good predictions for the pair correlation function of the uniform electron gas, in comparison to quantum Monte Carlo simulation [5]. The choice for the modified confining potential is described in Appendix B, where the potential is represented in terms of a "trial" quantum density imposing a known limit. Density profiles calculated on the basis of chosen quantum input are given in Secs. III and IV for values of t and r_s corresponding to the line $\Gamma = 20$ in Fig. 1. The purely classical profile would be the same in all of these cases since it depends only on Γ. Hence, the observed differences are purely quantum effects. Two choices for determination of the effective trap are explored here. The first is that where the trial density is the limit of noninteracting Fermions in a harmonic trap. At the highest values of t and r_s the classical limit is valid and at $\Gamma = 20$ Coulomb correlations are strong enough for shell structure, well-known for dusty plasmas [35]. At the smallest values of t and r_s a different shell structure emerges from extreme distortion of the noninteracting trial density due to exchange effects. The analysis for a second choice of the effective trap is repeated in Sec. IV with an improved trial density to include the effects of Coulomb interactions. With this quantum input, the new shell structure at small t and r_s no longer dominates and the quantum differences from the classical form are quantitative rather than qualitative. This sensitivity of the classical theory to the modifications of the confining potential, the need for guidance from simulation, and the outlook for future applications in materials sciences are discussed in the last section.

II. DENSITY PROFILE: CLASSICAL MAP OF THE QUANTUM SYSTEM

The Hamiltonian for N particles with charge q in a harmonic trap is

$$H - \mu N = \sum_{i=1}^{N} \frac{p_i^2}{2m} + \frac{1}{2}\sum_{i\neq j}^{N} \frac{q^2}{|\mathbf{r}_i - \mathbf{r}_j|} - \int d\mathbf{r}\mu(\mathbf{r})\widehat{n}(\mathbf{r}), \quad (1)$$

with the local chemical potential given explicitly as

$$\mu(\mathbf{r}) = \mu - \tfrac{1}{2}m\omega^2 r^2, \quad (2)$$

and the operator $\widehat{n}(\mathbf{r})$ representing the microscopic density is

$$\widehat{n}(\mathbf{r}) = \sum_{i=1}^{N} \delta(\mathbf{r} - \mathbf{q}_i). \tag{3}$$

The constant μ determines the average number of charges $\overline{N}$ at equilibrium in the grand-canonical ensemble. As a consequence of the harmonic potential, the equilibrium average density profile for the charges is nonuniform,

$$n(\mathbf{r},\beta \mid \mu) = \Omega^{-1} \sum_{N=1}^{\infty} N \int d\mathbf{r}_2 \cdots d\mathbf{r}_N \times \langle \mathbf{r} \cdots \mathbf{r}_N | e^{-\beta(H-\mu N)} | \mathbf{r} \cdots \mathbf{r}_N \rangle, \tag{4}$$

where $\langle \mathbf{r}_1 \cdots \mathbf{r}_N | X | \mathbf{r}_1 \cdots \mathbf{r}_N \rangle$ is the N particle diagonal, properly symmetrized (Fermions or Bosons) matrix element in coordinate representation and Ω is the grand potential,

$$\Omega(\beta \mid \mu) = \sum_{N=1}^{\infty} \int d\mathbf{r}_1 \cdots d\mathbf{r}_N \langle \mathbf{r}_1 \cdots \mathbf{r}_N | e^{-\beta(H-\mu N)} | \mathbf{r}_1 \cdots \mathbf{r}_N \rangle. \tag{5}$$

The notation $f(a,b \mid c)$ indicates a function of the parameters a,b and a functional of $c(\mathbf{r})$. The density profile in the classical limit has been studied in detail, via simulation and theory [16,17]. In that case the dimensionless form depends only on $\overline{N}$ and the Coulomb coupling constant $\Gamma = \beta q^2/r_0$. For sufficiently large Coulomb coupling, Γ, the formation of shell structure is observed in $n(\mathbf{r})$. The objective here is to exploit this classical description to explore the effects of quantum diffraction and exchange via a proposed equivalent classical system [3,4]. The equivalent classical system has an effective local chemical potential, $\mu_c(\mathbf{r})$, an effective pair potential, $\phi_c(|\mathbf{r}_i - \mathbf{r}_j|)$, and an effective inverse temperature, β_c. These must be given as functions of $\mu(\mathbf{r})$, $\phi(|\mathbf{r}_i - \mathbf{r}_j|)$, and β for the quantum system. Dimensionless quantities are used below such that the explicit form for β_c is not required.

The basis for the classical study used here is the hypernetted chain (HNC) description for an inhomogeneous equilibrium system [37], or Eq. (37) of Ref. [5],

$$\ln\left[n(\mathbf{r},\beta_c \mid \mu_c)\lambda_c^3\right] = \beta_c \mu_c(\mathbf{r}) + \int d\mathbf{r}' c^{(2)}(\mathbf{r},\mathbf{r}',\beta_c \mid \mu_c) n(\mathbf{r}'), \tag{6}$$

where $\lambda_c = (2\pi\beta_c\hbar^2/m)^{1/2}$ is the thermal de Broglie wavelength expressed in terms of the effective classical temperature, and $c^{(2)}(\mathbf{r},\mathbf{r}',\beta_c \mid \mu_c)$ is the direct correlation function defined by the Ornstein-Zernicke equation in terms of the pair correlation function for the inhomogeneous system [37]. Further details of the origins for this equation in classical density functional theory are given in Ref. [16]. The classical studies made a further approximation to this expression, replacing the direct correlation function for the inhomogeneous system by that for a corresponding uniform one-component plasma (OCP or jellium), $c^{(2)}(\mathbf{r},\mathbf{r}',\beta_c \mid \mu_c) \to c(|\mathbf{r} - \mathbf{r}'|,\beta_c,\mu_c)$. The results based on this approximation are found to be quite accurate except at very strong coupling. A partial theoretical basis for this approximation has been given [38], and it will be made here as well.

An equivalent Boltzmann form for the density is defined in terms of a dimensionless potential $U(\mathbf{r})$ defined by

$$n(\mathbf{r},\mu_c,\beta_c) = \overline{N} \frac{e^{-U(\mathbf{r},\mu_c,\beta_c)}}{\int d\mathbf{r}' e^{-U(\mathbf{r}',\mu_c,\beta_c)}}, \tag{7}$$

where (6) gives

$$U(\mathbf{r},\mu_c,\beta_c) = -\nu_c(\mathbf{r}) - \frac{\overline{N}}{\int d\mathbf{r}' e^{-U(\mathbf{r}',\mu_c,\beta_c)}} \times \int d\mathbf{r}' e^{-U(\mathbf{r}',\mu_c,\beta_c)} c(|\mathbf{r} - \mathbf{r}'|,\mu_c,\beta_c). \tag{8}$$

The dimensionless activity, $\nu_c(\mathbf{r},\mu_c,\beta_c) = \beta_c\mu_c(\mathbf{r})$, has been introduced in (8) and $c(r,\mu_c,\beta_c)$ is now the direct correlation function for the uniform OCP. For future reference, note that at fixed $\overline{N}$ the representation for $n(\mathbf{r})$ is invariant to a shift of $\nu_c(\mathbf{r})$ by a constant. In the following applications this flexibility will be used to choose $U(\mathbf{0},\mu_c,\beta_c) = 0$.

Equations (7) and (8) are a classical representation for the density profile (4) for the underlying quantum system. The latter is parametrized by the total average number of particles $\overline{N}$, the inverse temperature β, and the chemical potential of the uniform system μ. In the following, a change of variables from β,μ to $\beta,\overline{n}$ is considered, where $\overline{n}$ is the average density of the representative uniform system. To introduce the density, it is necessary to assign a volume for the system. This can be taken as the volume of a sphere with radius R_0 corresponding to a particle at the greatest distance from the center. At equilibrium the average fluid phase density is spherically symmetric so that the total average force on that particle is

$$\frac{(\overline{N}-1)q^2}{R_0^2} - m\omega^2 R_0 = 0, \quad \Rightarrow R_0^3 = (\overline{N}-1)\frac{q^2}{m\omega^2}. \tag{9}$$

This gives the average density to be

$$\overline{n} \equiv \frac{3\overline{N}}{4\pi R_0^3} = \frac{3m\omega^2}{4\pi q^2}\frac{\overline{N}}{\overline{N}-1}. \tag{10}$$

As expected, the density is determined by the trap parameter $m\omega^2/q^2$. A corresponding length scale r_0 is the average distance between particles given by $4\pi r_0^3/3 = 1/\overline{n}$. The following dimensionless measures of distance, temperature, and density will be used:

$$\mathbf{r}^* = \frac{r}{r_0}, \quad t = \frac{1}{\beta\epsilon_F}, \quad r_s = \frac{r_0}{a_b}. \tag{11}$$

Here ϵ_F is the Fermi energy and a_b is the Bohr radius, both defined in terms of the mass and charge of the particles in the trap:

$$\epsilon_F = \frac{1}{2m}\hbar^2(3\pi^2\overline{n})^{2/3} = \left(\frac{m_e}{m}\right)\epsilon_{eF}, \quad a_b = \frac{\hbar^2}{mq^2} = \left(\frac{m_e e^2}{mq^2}\right)a_B, \tag{12}$$

$$\nu(\mathbf{r},\mu_e,\beta) = \beta\mu_e - \frac{1}{2}\Gamma(t,r_s)r^{*2}. \tag{13}$$

In the last equalities of (12) ϵ_{eF} and a_B are the electron Fermi energy and the usual Bohr radius, respectively. The prefactor $m_e e^2/mq^2$ shows how the very large values of r_s in Fig. 1 can be obtained for particles of large mass and large charge.

Finally, define the reduced potential $u(\mathbf{r}^*,t,r_s)$, direct correlation function $\overline{c}(r^*,t,r_s)$, and local activity $\overline{\nu}_c(\mathbf{r}^*,t,r_s)$ by

$$\begin{aligned} U(\mathbf{r}) &= \Gamma_e(t,r_s)u(\mathbf{r}^*,t,r_s),\\ c(r,\mu_c,\beta_c) &= \Gamma_e(t,r_s)\overline{c}(r^*,t,r_s),\\ \nu_c(\mathbf{r},\mu_c,\beta_c) &= \Gamma_e(t,r_s)\overline{\nu}_c(\mathbf{r}^*,t,r_s). \end{aligned} \tag{14}$$

An effective coupling constant $\Gamma_e(t,r_s)$ has been extracted in each case:

$$\Gamma_e(t,r_s) = \frac{2}{\beta\hbar\omega_p \coth(\beta\hbar\omega_p/2)}\Gamma, \quad \Gamma \equiv \frac{\beta q^2}{r_0}. \tag{15}$$

Here $\omega_p = \sqrt{4\pi\overline{n}q^2/m}$ is the plasma frequency. The dimensionless parameter is $\beta\hbar\omega_p = (4/3)(2\sqrt{3}/\pi^2)^{1/3}\sqrt{r_s}/t \simeq 0.940\,52\sqrt{r_s}/t$. At fixed r_s and large t, $\Gamma_e(t,r_s) \to \Gamma \simeq 0.543 r_s/t$, which is the classical Coulomb coupling constant. The motivation for introducing $\Gamma_e(t,r_s)$ is the fact that it represents the strength of the Coulomb tail for the effective classical pair potential [4], as shown in Appendix A, Eq. (A5). This means that the strength of the effective classical repulsion of particles in the trap is $\Gamma_e(t,r_s)$, while the strength of the harmonic containment is $\Gamma(t,r_s)$ [see (13)]. Since $\Gamma_e(t,r_s)$ decreases with increasing quantum effects, stronger confinement relative to the purely classical result is expected.

The dimensionless form for the density profile, from (7) and (8) is now

$$n^*(\mathbf{r}^*,t,r_s) = n(\mathbf{r},\mu_c,\beta_c)r_0^3 = \overline{N}\frac{e^{-\Gamma_e(t,r_s)u(\mathbf{r}^*,t,r_s)}}{\int d\mathbf{r}^{*\prime}e^{-\Gamma_e(t,r_s)u(\mathbf{r}^{*\prime},t,r_s)}}, \tag{16}$$

$$\begin{aligned} u(\mathbf{r}^*,t,r_s) = -\overline{\nu}_c(\mathbf{r}^*,t,r_s) - \frac{\overline{N}}{\int d\mathbf{r}^{*\prime\prime}e^{-\Gamma_e(t,r_s)u(\mathbf{r}^{*\prime\prime},t,r_s)}}\\ \times \int d\mathbf{r}^{*\prime}e^{-\Gamma_e(t,r_s)u(\mathbf{r}^{*\prime},t,r_s)}\overline{c}(|\mathbf{r}^*-\mathbf{r}^{*\prime}|,t,r_s). \end{aligned} \tag{17}$$

Practical application requires specification of the direct correlation function $\overline{c}(r^*,t,r_s)$ for jellium and the classical activity $\overline{\nu}_c(r^*,t,r_s)$. The method for determining these is such that they are explicit functions of the dimensionless variables t,r_s for the given quantum system, rather than of the associated classical parameters μ_c,β_c. Hence the potentially confusing notation in (14). The former is determined from an accurate equivalent classical calculation described elsewhere [5] and summarized in Appendix A. The direct correlation function is a classical concept whose quantum modifications here appear only through the effective pair potential. That potential is obtained in Appendix A and has two main changes from the underlying Coulomb potential due to quantum effects in the classical representation. The first is a regularization of the Coulomb singularity at the origin due to diffraction effects; the pair potential remains finite at zero separation. The second main change is the strength of the $1/r$ behavior at large distances, with the coupling constant Γ being replaced with Γ_e of (15).

The activity $\overline{\nu}_c(\mathbf{r}^*,t,r_s)$ describes the effective classical trap potential corresponding to the actual quantum harmonic trap, and its approximate determination is described in Appendix B. It is defined such that the density profile for a chosen quantum system is recovered in an appropriate limit. In this way the exact quantum effects of that limit are incorporated in the classical system and exploited approximately away from that limit as well. The resulting form for (16) and (17) obtained in Appendix B is

$$n^*(\mathbf{r}^*,t,r_s) = N\frac{n_T^*(\mathbf{r}^*,t,r_s)e^{\Gamma_e(t,r_s)\Delta u(\mathbf{r}^*,t,r_s|n)}}{\int d\mathbf{r}' n_T^*(\mathbf{r}^{*\prime})e^{\Gamma_e(t,r_s)\Delta u(\mathbf{r}^{*\prime},t,r_s|n)}}. \tag{18}$$

$$\begin{aligned} \Delta u(\mathbf{r}^*,t,r_s \mid n) = \int d\mathbf{r}'[\overline{c}(|\mathbf{r}^*-\mathbf{r}^{*\prime}|,t,r_s)n^*(\mathbf{r}^{*\prime},t,r_s)\\ -\overline{c}_T(|\mathbf{r}^*-\mathbf{r}^{*\prime}|,t,r_s)n_T^*(\mathbf{r}',t,r_s)]. \end{aligned} \tag{19}$$

Here $n_T^*(\mathbf{r}^*,t,r_s)$ is the "trial" quantum density profile enforcing the associated quantum limit for $n^*(\mathbf{r}^*,t,r_s)$, and $\overline{c}_T(r^*,t,r_s)$ is the associated direct correlation function for that limit. See Appendix B for further details. Equations (18) and (19) are the basis for all the results reported here. Two cases are considered here, the limit of noninteracting Fermions in a harmonic trap and the corresponding system with weak Coulomb interactions.

III. CLASSICAL TRAP FOR NONINTERACTING FERMIONS

For a first study of the quantum effects consider an effective trap whose classical density is the same as the quantum density of noninteracting Fermions in a harmonic trap. The corresponding trap density in (18) and (19) is denoted by $n_T^*(r^*,t,r_s) \to n^{*(0)}(r^*,t,r_s)$ and the direct correlation function for this case is denoted by $c_T(r^*,t,r_s) \to c^{(0)}(r^*,t,r_s)$. The former is calculated directly from

$$n^{*(0)}(\mathbf{r}^*,t,r_s) = 2r_0^3\langle\mathbf{r}|\left\{e^{[\beta\frac{\hat{p}^2}{2m}-(\nu_0-\frac{1}{2}m\omega^2\hat{r}^2)]}+1\right\}^{-1}|\mathbf{r}\rangle. \tag{20}$$

$\langle\mathbf{r}|X|\mathbf{r}\rangle$ denotes a diagonal matrix element in coordinate representation. It has been assumed that the system is composed of unpolarized spin-$\frac{1}{2}$ particles. A caret on a variable indicates it is the operator corresponding to that variable. The parameter ν_0 is determined by the condition that the total average number of particles is the same as the interacting system:

$$\overline{N}(t,r_s) = 2r_0^{-3}\int d\mathbf{r}\langle\mathbf{r}|\left\{e^{[\beta\frac{\hat{p}^2}{2m}-(\nu_0-\frac{1}{2}m\omega^2\hat{r}^2)]}+1\right\}^{-1}|\mathbf{r}\rangle. \tag{21}$$

Equations (20) and (21) can be evaluated in terms of the harmonic oscillator eigenfunctions and eigenvalues. Instead, here a local density (Thomas-Fermi) approximation is used. This follows from the replacement of the operator $\hat{r}^2$ by the corresponding c-number r^2. Then the matrix element can be evaluated to give

$$n^{*(0)}(\mathbf{r}^*) \to \left(\frac{r_0}{\lambda}\right)^3\frac{4}{\sqrt{\pi}}I_{\frac{1}{2}}\left[\nu_0-\frac{1}{2}\Gamma(t,r_s)r^{*2}\right], \tag{22}$$

$$\overline{N} = \left(\tfrac{r_0}{\lambda}\right)^3 4\pi\int_0^\infty dr^*r^{*2}\tfrac{4}{\sqrt{\pi}}I_{\frac{1}{2}}\left\{\left[\nu_0-\tfrac{1}{2}\Gamma(t,r_s)r^{*2}\right]\right\}. \tag{23}$$

The Fermi function $I_\alpha(\beta\mu)$ and thermal de Broglie wavelength λ are given by

$$I_\alpha(\beta\mu) = \int_0^\infty dx \frac{x^\alpha}{e^{x-\beta\mu}+1}, \quad \lambda = \left(\frac{2\pi\hbar^2\beta}{m}\right)^{1/2}. \quad (24)$$

The validity of this Thomas-Fermi approximation for the conditions considered here ($\overline{N} = 100$) is demonstrated in Appendix C.

The direct correlation function $c^{(0)}(r^*,t,r_s)$ is nontrivial because the classical system corresponding to a noninteracting quantum gas has pairwise interactions needed to reproduce the symmetrization effects. Hence, calculation of properties for this effective classical system is a true many-body problem. The Ornstein-Zernicke equation is used, with the known exact quantum noninteracting pair correlation function $g^{(0)}(r)$ as input [4]:

$$c^{(0)}(r^*,t,r_s) = [g^{(0)}(r^*,t,r_s) - 1] - \overline{n} \int \times d\mathbf{r}^{*\prime} c^{(0)}(|\mathbf{r}^* - \mathbf{r}^{*\prime}|,t,r_s)[g^{(0)}(r^{*\prime},t,r_s) - 1]. \quad (25)$$

Finally, the direct correlation function for the interacting system is calculated from the coupled HNC and Ornstein-Zernicke equations:

$$\ln[g(r^*,t,r_s)] = -\phi_c^*(r^*,t,r_s) + [g(r^*,t,r_s) - 1] - c(r^*,t,r_s), \quad (26)$$

$$c(r^*,t,r_s) = [g(r^*,t,r_s) - 1] - \overline{n} \int d\mathbf{r}' c(|\mathbf{r}^* - \mathbf{r}^{*\prime}|,t,r_s)[g(r^{*\prime},t,r_s) - 1]. \quad (27)$$

Here $\phi_c^*(r^*,t,r_s)$ is the effective classical pair interaction representing the uniform electron gas, described in Appendix A.

Equations (18) and (19) for this case are now

$$n^*(r^*,t,r_s) = N \frac{n^{*(0)}(r^*,t,r_s)e^{\Gamma_e(t,r_s)\Delta u(r^*,t,r_s|n)}}{\int d\mathbf{r}' n^{*(0)}(r^{*\prime})e^{\Gamma_e(t,r_s)\Delta u(\mathbf{r}^{*\prime},t,r_s|n)}}, \quad (28)$$

$$\Delta u(\mathbf{r}^*,t,r_s \mid n) = \int d\mathbf{r}'[\overline{c}(|\mathbf{r}^* - \mathbf{r}^{*\prime}|,t,r_s)n^*(r^{*\prime},t,r_s) - \overline{c}^{(0)}(|\mathbf{r}^* - \mathbf{r}^{*\prime}|,t,r_s)n^{*(0)}(r^{*\prime},t,r_s)]. \quad (29)$$

The quantum input for this classical description is twofold. The first is a modification of the Coulomb interactions among charges via $\phi_c^*(r^*,t,r_s)$, due to both diffraction and exchange effects. These occur through the direct correlations $\overline{c}(r^*,t,r_s)$. Additional quantum effects occur due to the modification of the shape and intensity of the harmonic trap. These occur through $n^{*(0)}(r^*,t,r_s)$. To explore these effects, a series of density profiles is shown in Fig. 2 for values of t,r_s corresponding to the line $\Gamma = 20$ in Fig. 1. Without quantum effects all profiles would be the same as the classical limit shown. The observed classical shell structure in that case is due entirely to strong Coulomb coupling with no quantum effects. As the values of t,r_s are decreased this Coulomb shell is distorted and shifted inward, corresponding to a weakening of the Coulomb repulsion through a decreasing effective coupling $\Gamma_e(t,r_s)$. This weakening of Coulomb correlations

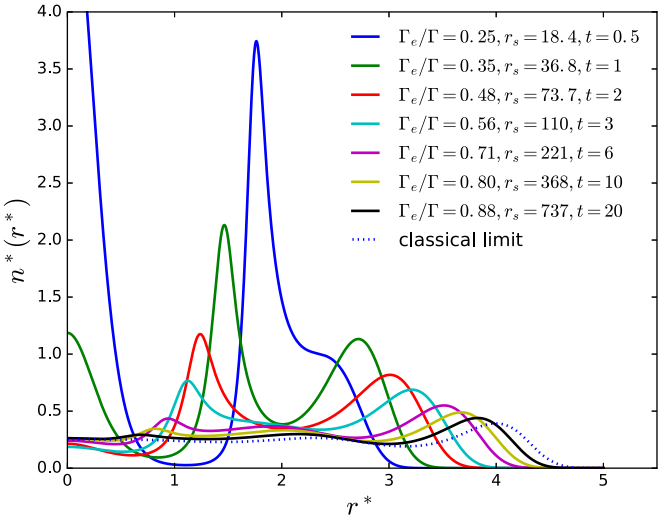

FIG. 2. Onset of quantum effects for a system of 100 particles. Here $\Gamma = 20$ as temperature decreases from $t = 20$ (lowest peak) to $t = 0.5$ (highest peak).

in $c(r^*,t,r_s)$ is displayed in Fig. 3(a). The direct correlation function has quantum effects that enter the HNC theory only through the effective pair potential (Appendix A). The latter has a Coulomb tail whose amplitude is decreased by Γ_e/Γ so that long-range correlations are weakened. At shorter distances the Coulomb singularity is removed in the effective pair potential due to diffraction effects. The classical direct correlation function is finite at $\mathbf{r}^* = 0$ for sufficiently strong coupling due to Coulomb correlations in spite of the singular Coulomb potential. However, with quantum diffraction effects the effective pair potential is nonsingular and the direct correlation function remains finite at $\mathbf{r}^* = 0$ even at weak coupling. These qualitative changes are illustrated for three cases in Fig. 3(a) corresponding to $t = 200,\ 20$, and 2 in Fig. 2. The smaller values at $\mathbf{r}^* = 0$ tend to enhance shell formation, while the weaker coupling of Γ_e/Γ tends to decrease it.

A qualitatively new consequence of quantum effects occurs at the lowest value of $t = 0.5$ and $r_s = 18.4$. A strong single shell occurs that is unrelated to the classical Coulomb shell structure and is due entirely to a change in shape of the confining potential. To be more explicit, write the confining potential, or equivalently $\overline{v}_c(\mathbf{r}^*,t,r_s)$, as

$$\overline{v}_c^{(0)}(\mathbf{r}^*,t,r_s) - \overline{v}_c^{(0)}(\mathbf{0},t,r_s) = \frac{\Gamma}{\Gamma_e}\frac{1}{2}\mathbf{r}^{*2} + \Delta(\mathbf{r}^*,t,r_s). \quad (30)$$

There are two quantum effects evident in this form, an increase in amplitude of the harmonic potential by Γ/Γ_e and a change in shape represented by $\Delta(\mathbf{r}^*,t,r_s)$. The change in amplitude of the harmonic potential is a reflection of its enhancement relative to $\overline{c}(r^*,t,r_s)$ and is largely responsible for the increased confinement observed in all density profiles of Fig. 2. As the shells are pulled inwards, this also tends to cause a population transfer to the outer shell. However, at the lowest temperatures the change in shape from the harmonic form becomes large. It is this distortion that is responsible for the onset of the new shell structure seen in Fig. 2. This is confirmed in Fig. 4, which shows the superposition of the shell and the local distortion of the confining potential relative to its harmonic form. The origin

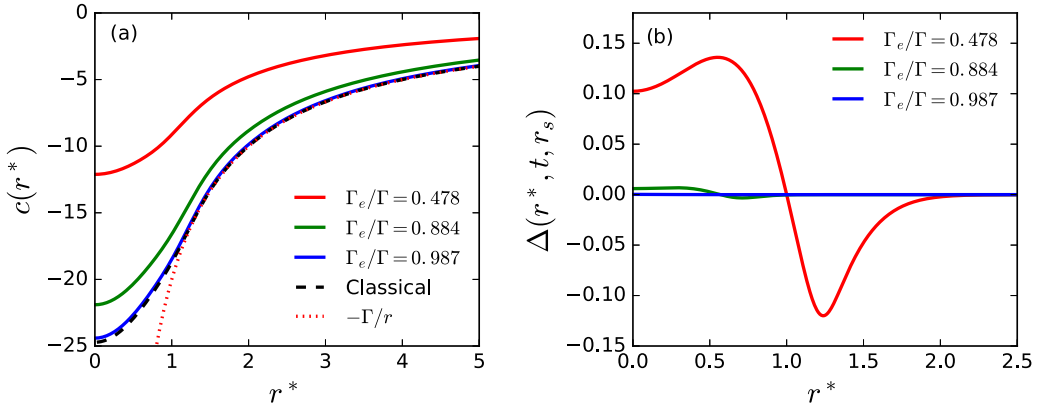

FIG. 3. Two quantum effects for $\Gamma = 20$. (a) Quantum effect on the direct correlation function. The ratio Γ_e/Γ varies from 0.478 (upper solid line) to 0.987 (lower solid line). The negative of the Coulomb potential is also shown for reference. (b) Quantum effect on the shape of the trapping potential near the origin for the same conditions. The red (highest-peaked) line shows the effect increases as Γ_e/Γ decreases.

of this distortion is the Fermi statistics of the noninteracting particles, which force the trap density to go to zero at a finite radius as $t \to 0$ (Appendix B). This translates into a hard wall for the effective confining potential and an associated shell structure (even in a classical fluid hard wall confinement leads to shell structure). The predicted location of the $t = 0$ wall in Appendix B is 1.77, very close to that observed in Fig. 4 at $t = 0.5$.

IV. CLASSICAL TRAP WITH WEAK COULOMB INTERACTIONS

Now consider the same analysis based on (18) and (19), but with a better choice for the effective confining potential to include some quantum effects of the Coulomb interactions on the effective classical confining potential. This change does not affect $\overline{c}(r^*,t,r_s)$, which is the same as in the previous section. The new choice is defined by imposing a weak-coupling limit for which the corresponding trap density is obtained from a quantum density functional calculation including Hartree and exchange interactions in a local density approximation, $n_T^*(\mathbf{r}^*,t,r_s) \to n^{*(w)}(\mathbf{r}^*,t,r_s)$ given by (B17). The details are discussed in Appendix B 2 . Accordingly, the corresponding classical limit for the trial direct correlation function is its weak-coupling expansion to first order in Γ, $\overline{c}_T(r^*,t,r_s) \to \overline{c}^{(0)}(r^*,t,r_s) + \Gamma\overline{c}^{(1)}(r^*,t,r_s)$, and (18) and (19) become

$$n^*(\mathbf{r}^*,t,r_s) = \overline{N}\frac{n^{*(w)}(\mathbf{r}^*,t,r_s)e^{\Gamma_e(t,r_s)\Delta u(\mathbf{r}^*,t,r_s|n)}}{\int d\mathbf{r}' n^{*(w)}(\mathbf{r}^{*\prime})e^{\Gamma_e(t,r_s)\Delta u(\mathbf{r}^{*\prime},t,r_s|n)}}. \tag{31}$$

$$\begin{aligned}\Delta u(\mathbf{r}^*,t,r_s \mid n) = \int d\mathbf{r}'\{&\overline{c}(|\mathbf{r}^*-\mathbf{r}^{*\prime}|,t,r_s)n^*(\mathbf{r}^{*\prime},t,r_s) \\ &- [\overline{c}^{(0)}(|\mathbf{r}^*-\mathbf{r}^{*\prime}|,t,r_s) \\ &+ \Gamma\overline{c}^{(1)}(|\mathbf{r}^*-\mathbf{r}^{*\prime}|,t,r_s)]n^{*(w)}(\mathbf{r}',t,r_s)\}.\end{aligned} \tag{32}$$

The direct correlation functions $\overline{c}(r^*,t,r_s)$ and $\overline{c}^{(0)}(r^*,t,r_s)$ are again calculated in the HNC approximation using (25)–(27). Also, the weak coupling coefficient $\overline{c}^{(1)}(r^*,t,r_s)$ is obtained numerically from these equations for asymptotically small Γ.

Figure 5 shows the density profiles for the same temperatures as in Fig. 2 along the line $\Gamma = 20$ in Fig. 1. The results are quite similar at the high temperatures, e.g., $t = 20$, as the classical limit is approached. However, at all lower temperatures there is a qualitative difference between Figs. 5 and 2. In the latter case the intermediate peak diminishes and the new shell at small r^* grows as the temperature decreases until a single dominant peak is formed at the lowest temperature. In contrast, the outer and intermediate peaks of Fig. 5 change in a unified fashion as the overall density profile contracts with decreasing temperature. The two-peak structure is maintained with only quantitative changes occurring due to quantum effects; no new shell structure is seen as in Fig. 2. As indicated in (30), the quantum effects on the confining potential are an enhancement of the harmonic form and a distortion of that form. The distortion $\Delta(\mathbf{r}^*,t,r_s)$ is now very much decreased by the inclusion of weak Coulomb interactions in the determination of the classical confining potential, eliminating the new "hard-wall" shell structure of Fig. 2. This is illustrated in Fig. 6 for $t = 0.5$.

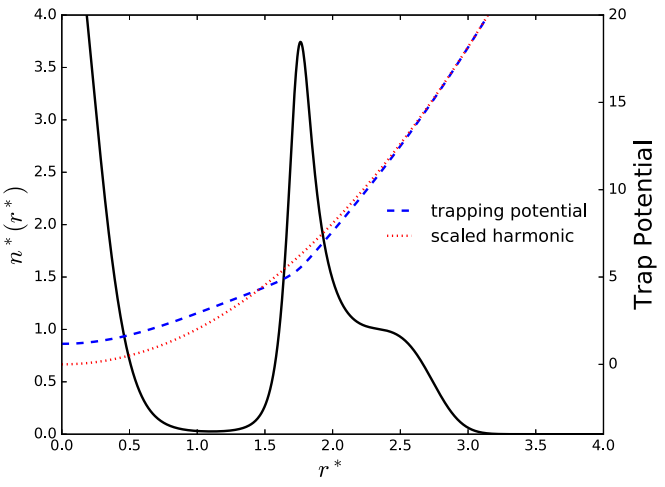

FIG. 4. The low-temperature quantum effect of the trapping potential on the density $n(r)$. The system is strongly coupled ($\Gamma = 20$), with $r_s = 18.4$ and $t = 0.5$. The scaled harmonic function is shown, as well as the full trapping potential.

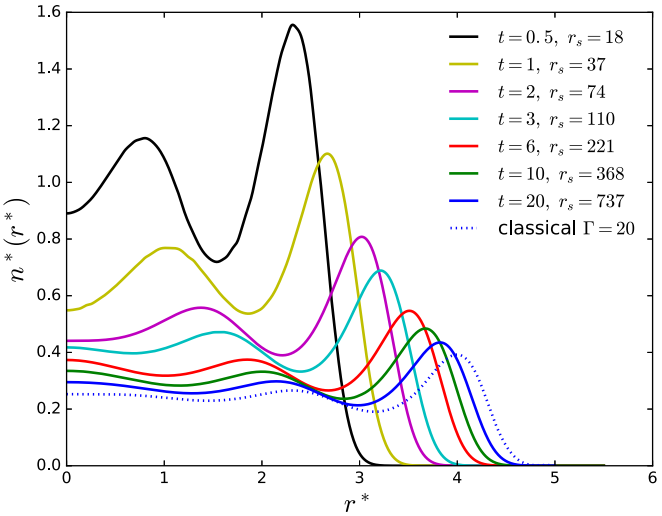

FIG. 5. Onset of quantum effects for a system of 100 particles. Here $\Gamma = 20$ as temperature decreases from $t = 20$ (lowest peaks) to $t = 0.5$ (highest peaks).

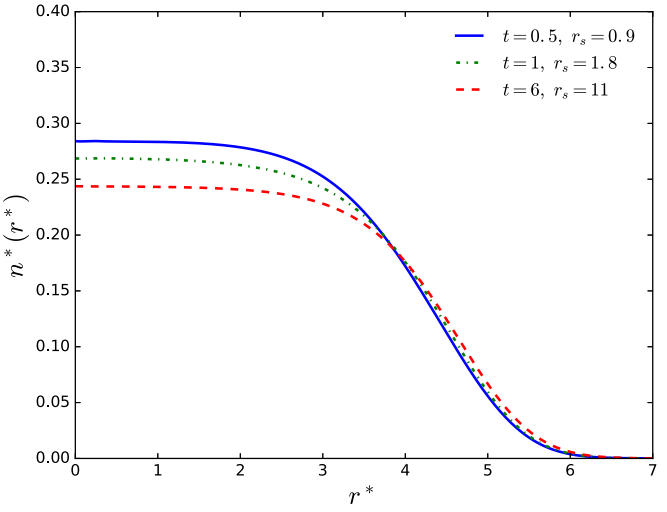

FIG. 7. Density profiles for low temperatures ($t = 0.5,1,6$) at $\Gamma = 1$ for weak Coulomb interactions. No shell structure is formed at small temperatures for the weakly coupled case.

The quantum effects on the amplitude and location of the shells in Fig. 5 are quite significant. For example, at $t = 1$ the outer peak increases by a factor of 2.8 relative to the classical value. The contraction is largely due to the factor $\Gamma(t,r_s)/\Gamma_e(t,r_s)$, which changes from 1.13 at $t = 20$ to 2.86 at $t = 1$.

The results discussed thus far are all for the strong-coupling condition $\Gamma = 20$. This was chosen because shell structure is present for these conditions even in the classical limit. It is instructive now to consider the case $\Gamma = 1$ for which there is no classical shell structure. Figure 7 shows the results for $t = 6$, 1, and 0.5. In contrast to the strong-coupling case, $t = 6$ is very close to the classical limit. The contraction of the profile

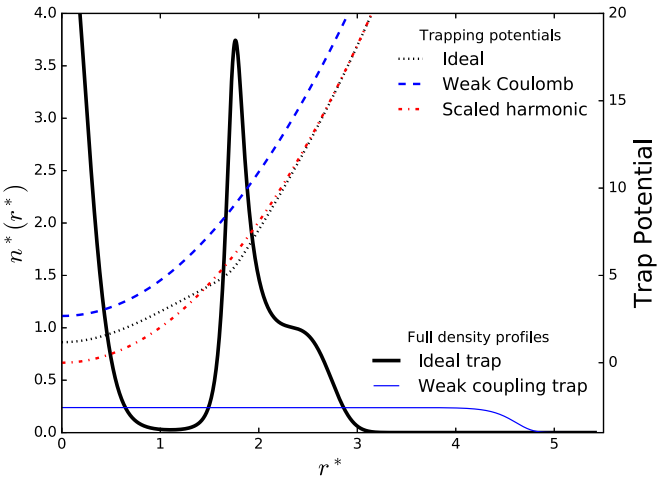

FIG. 6. Effect of including weak Coulomb interactions on trapping potential distortion. The black dotted line is the distorted trapping potential for noninteracting particles. The blue dashed line is the distorted trapping potential when weak Coulomb interactions are included. For reference, the red dashed-dotted line shows the scaled harmonic potential $\frac{1}{2}\frac{\Gamma}{\Gamma_e}r^{*2}$ with no shape distortion. Here $t = 0.5$ and $\Gamma = 20$.

is the dominant quantum effect at lower temperatures, and there is no shell structure evident in any case.

V. DISCUSSION

The classical shell structure for strong-coupling conditions in the upper right corner of Fig. 1 has provided a wealth of insight into formation of shell structure due to Coulomb correlations. Here these studies have been extended in the direction of additional quantum effects. The method chosen, an equivalent classical system, allows inclusion of the diverse quantum effects into an extension via effective pair potentials and effective confinement potentials. The quantum effects are included in the modification of these potentials from their classical Coulomb and harmonic forms in a controlled way defined by the formalism of Refs. [3,4]. Two approximate implementations of that formalism have been described. In both, the pair correlations among charges expressed by the direct correlation function $\overline{c}(r^*,t,r_s)$ are calculated from the classical HNC liquid-state theory, known to be accurate for strong correlations, e.g., $\Gamma = 20$. The qualitative effects of quantum mechanics are illustrated in Fig. 3(a). The first approximation for the effective confining potential is that which gives the exact quantum density profile for noninteracting charges. The result is a scaling of the original harmonic trap by a factor $\Gamma(t,r_s)/\Gamma_e(t,r_s)$, which tends to increase the confinement relative to the Coulomb correlations. In addition there is a distortion of the harmonic form at low temperatures that produces a "hard wall" associated with the vanishing of the noninteracting density at a finite value of r^*. This leads to a new shell structure not related to Coulomb correlations.

The second choice for the confining potential, described in Sec. IV, is that which gives the density profile for a weak coupling quantum density functional calculation. This potential includes the effects of Coulomb interactions. It has a similar scaling of the harmonic form, but no longer shows the strong distortion [compare Figs. 3(b) and 6] and hence no new shell structure. In fact, the profiles of Fig. 5 at $\Gamma = 20$ appear

like a self-similar contraction constrained by the normalization to $\overline{N} = 100$. The choice of parameters $\Gamma = 20, \overline{N} = 100$ was made to ensure multiple shells in the reference classical limit. The brief consideration of $\Gamma = 1, \overline{N} = 100$ in Fig. 7 confirms that there is no new shell structure induced solely by quantum effects.

Clearly, there is more to be done with this classical description of a quantum system, such as $t < 0.5$ and much smaller $\overline{N}$ to make direct connection with the literature quoted in the Introduction on quantum dots and ultracold gases, for example. Models for such experimental situations should involve a straightforward application of the method studied here. Focus on other properties such as spin polarization or coherent control of trap properties, charge dependence and others acceptable to direct observation can be addressed. For example, simple dynamical modes can be identified (a novel "spectroscopy" based on a quantum breathing mode has been proposed recently [39,40]). Smaller particle number and access to details of optical properties will require a more detailed specification of the quantum input, beyond Thomas-Fermi. A different direction for application of the results here is obtained by the replacement of the harmonic trap with a Coulomb potential to calculate the electron distribution about an ion. Although this is, of course, a solved problem of quantum chemistry, its extension to a random configuration of ions is of intense current interest for warm, dense-matter applications. The current interest in that case is application of density functional theory for the electron density in the presence of such an ion configuration. Such densities are required to compute the forces in quantum molecular dynamics simulations for the ions in warm, dense matter at finite temperatures where traditional density functional methods fail [1]. The traditional approach has a bottleneck in the solution of the Kohn-Sham self-consistent equations [1] for temperatures near the Fermi temperature. Here those self-consistent equations are replaced with the classical integral equations of HNC. This advantage has been stressed recently by Dharma-wardana [31,32].

ACKNOWLEDGMENTS

The authors are indebted to Michael Bonitz for his comments on an earlier draft. This research has been supported by DOE(USA) Grants No. DE-SC0002139 and No. DE-FG02-07ER54946.

APPENDIX A: EFFECTIVE CLASSICAL DIRECT CORRELATION FUNCTION

The density profile for charges in a trap is governed by both the confining potential and the correlations among the particles in the trap. The latter appear in (19) via the direct correlation function $c(r,\mu_c,\beta_c) = \Gamma_e(t,r_s)\overline{c}(r^*,t,r_s)$. In this appendix, the approximate evaluation of these correlations from the HNC integral equations of liquid-state theory [25] using an effective pair potential is summarized.

As noted in Sec. II, the correlations for the nonuniform charges in the trap are approximated by those for a uniform electron gas. The calculation of these correlations from an effective classical system has been described in some detail elsewhere [3], so only the relevant equations are reproduced here for completeness. The approximate effective pair potential used there is

$$\phi_c^*(r^*,t,r_s) = \beta_c\phi_c(r) = \phi_c^{*(0)}(r^*,t,r_s) + \frac{1}{n}\int \frac{d\mathbf{k}}{(2\pi)^3} e^{-i\mathbf{k}\cdot\mathbf{r}}\left[\frac{1}{S^{RPA}(k)} - \frac{1}{S^{(0)}(k)}\right]. \tag{A1}$$

Here $S^{RPA}(k)$ and $S^{(0)}(k)$ are the static structure factor for the random phase approximation and ideal gas, respectively. The first term $[\beta_c\phi_c(r)]^{(0)}$ is the effective potential for the ideal quantum gas obtained by inverting the coupled ideal gas HNC equations [25]; i.e., Eqs. (26) and (27) specialized to the ideal gas,

$$\ln[g^{(0)}(r^*,t,r_s)] = -\phi_c^{*(0)}(r^*,t,r_s) + [g^{(0)}(r^*,t,r_s) - 1] - c^{(0)}(r^*,t,r_s), \tag{A2}$$

$$c^{(0)}(r^*,t,r_s) = [g^{(0)}(r^*,t,r_s) - 1] - \overline{n}\int d\mathbf{r}' c^{(0)}(|\mathbf{r}^* - \mathbf{r}^{*\prime}|,t,r_s)[g^{(0)}(r^{*\prime},t,r_s) - 1], \tag{A3}$$

using the known exact ideal gas pair correlation function for $g^{(0)}(r,t,r_s)$. Finally, with $\phi_c^*(r^*,t,r_s)$ determined in this way the direct correlation function for the interacting system is calculated from the full coupled HNC equations (26) and (27).

As a practical matter, a simplified representation of (A1) has been proposed [5]. The ideal gas contribution $\phi_c^{*(0)}(r^*,t,r_s)$ is the same, but the contribution from the Coulomb interactions is modeled by the exact low-density, weak-coupling functional form first derived by Kelbg [43]. Here that form is parametrized to include the exact low-density value for the pair correlation function at $r = 0$ [44] and the large r behavior of the more complete form (A1):

$$\phi_c^*(r^*,t,r_s) \simeq \phi_c^{*(0)}(r^*,t,r_s) + \Delta_K^*(r^*,\Gamma_e,r_s), \tag{A4}$$

with

$$\Delta_K^*(r^*,\Gamma_e,r_s) \equiv \frac{\Gamma_e}{r^*}\left\{1 - \exp[-(ar^*)^2] + \sqrt{\pi}\frac{ar^*}{\gamma}\,\mathrm{erfc}(\gamma ar^*)\right\}. \tag{A5}$$

Here

$$a = (r_s/\Gamma_e)^{1/2}, \quad \gamma(\Gamma_e r_s) = -\frac{(\pi\Gamma_e r_s)^{1/2}}{\ln s(\Gamma_e r_s)}, \tag{A6}$$

and $s(\Gamma_e r_s)$ is the two-electron relative coordinate Slater sum at $r^* = 0$:

$$s(\Gamma_e r_s) = -4(\pi\Gamma_e r_s)^{1/2}\int_0^\infty dy e^{-y^2}\frac{y}{1 - e^{\pi(\Gamma_e r_s)^{1/2}/y}}. \tag{A7}$$

Also Γ_e is the effective coupling constant of (15). Clearly, (A4) has the computational advantage that $\Delta_K^*(r^*,\Gamma_e,r_s)$ is an explicit, analytic function of the input parameters t,r_s. The results obtained for correlations using (A4) are quite similar to those obtained using (A1).

APPENDIX B: EFFECTIVE CLASSICAL TRAP POTENTIAL

The effective classical description of the local density for charges confined in a harmonic trap is given by [3,4]

$$\ln\left[n(\mathbf{r})\lambda_c^3\right] = [\beta_c\mu_{ec} - \beta_c v_c(\mathbf{r})] + \int d\mathbf{r}' c(|\mathbf{r}-\mathbf{r}'|,\mu_c,\beta_c)n(\mathbf{r}'), \quad \text{(B1)}$$

where $n(\mathbf{r})$ is the desired charge density and $c(|\mathbf{r}-\mathbf{r}'|,\mu_c,\beta_c)$ is the direct correlation function for the homogeneous electron gas calculated as described in Appendix A. To complete the description, it is necessary to choose the effective trap potential and chemical potential, i.e., $[\beta_c\mu_{ec} - \beta_c v_c(\mathbf{r})]$. This is done by requiring that the effective trap reproduce a chosen approximate quantum density valid in some limit. In this way, some limiting quantum information is provided via the effective trap.

It is useful to express (B2) in the equivalent form (7) that includes the normalization explicitly:

$$n(\mathbf{r},\mu_c,\beta_c) = \overline{N}\frac{e^{-U(\mathbf{r},\mu_c,\beta_c)}}{\int d\mathbf{r}' e^{-U(\mathbf{r}',\mu_c,\beta_c)}}, \quad \text{(B2)}$$

$$U(\mathbf{r},\mu_c,\beta_c) = -v_c(\mathbf{r},\mu_c,\beta_c) - \frac{\overline{N}}{\int d\mathbf{r}' e^{-U(\mathbf{r}',\mu_c,\beta_c)}} \times \int d\mathbf{r}' e^{-U(\mathbf{r}',\mu_c,\beta_c)} c(|\mathbf{r}-\mathbf{r}'|,\mu_c,\beta_c). \quad \text{(B3)}$$

Recall the notation that $v_c(\mathbf{r},\mu_c,\beta_c) = \beta_c\mu_c(\mathbf{r}) = \beta_c\mu_{ec} - \beta_c v_c(\mathbf{r})$.

Let $[\beta_c\mu_{ec} - \beta_c v_c(\mathbf{r})]_T$ denote the effective trap potential and chemical potential in some chosen limit. The density profile in that limit, $n_T(\mathbf{r},\mu_c,\beta_c)$, is therefore

$$\ln\left[n_T(\mathbf{r},\mu_c,\beta_c)\lambda_c^3\right] = [\beta_c\mu_{ec} - \beta_c v_c(\mathbf{r})]_T + \int \times d\mathbf{r}' c_T(|\mathbf{r}-\mathbf{r}'|,\mu_c,\beta_c)n_T(\mathbf{r}',\mu_c,\beta_c). \quad \text{(B4)}$$

Here $c_T(r,\mu_c,\beta_c)$ is the direct correlation function corresponding in the classical form to the quantum limit considered. The limit must be such that an independent quantum calculation of $n_T(\mathbf{r},\mu_c,\beta_c)$ can be implemented practically, and the corresponding $c_T(r,\mu_c,\beta_c)$ can be identified. Then with $c_T(r,\mu_c,\beta_c)$ and $n_T(\mathbf{r},\mu_c,\beta_c)$ known, Eq. (B4) defines the effective classical trap that gives the exact quantum density in the limit considered. The choice for the approximate effective trap in (B1) is now made as

$$[\beta_c\mu_{ec} - \beta_c v_c(\mathbf{r})] \to [\beta_c\mu_{ec} - \beta_c v_c(\mathbf{r})]_T. \quad \text{(B5)}$$

This assures the exact behavior $n_T(\mathbf{r},\mu_c,\beta_c)$ is recovered in the appropriate limit. With this choice (B2) and (B3) become

$$n(\mathbf{r},\mu_c,\beta_c) = N\frac{n_T(\mathbf{r},\mu_c,\beta_c)e^{\Delta U(\mathbf{r},\mu_c,\beta_c|n)}}{\int d\mathbf{r}' n_T(\mathbf{r}')e^{\Delta U(\mathbf{r}',\mu_c,\beta_c|n)}}. \quad \text{(B6)}$$

$$\Delta U(\mathbf{r},\mu_c,\beta_c \mid n) = \int d\mathbf{r}'[c(|\mathbf{r}-\mathbf{r}'|,\mu_c,\beta_c)n(\mathbf{r}',\mu_c,\beta_c) - c_T(|\mathbf{r}-\mathbf{r}'|,\mu_c,\beta_c)n_T(\mathbf{r}',\mu_c,\beta_c)]. \quad \text{(B7)}$$

Here it has been required that $\int d\mathbf{r} n_T(\mathbf{r},\mu_c,\beta_c) = \overline{N}$. Equations (18) and (19) are the dimensionless forms of (B6) and (B7) quoted in the text.

1. Noninteracting charges limit

The simplest choice for an imposed limit by the confining potential is that for noninteracting charges in a harmonic trap. This choice properly includes the nonclassical effects of exchange symmetry. The density in this case $n_T^*(r^*,t,r_s) \to n^{*(0)}(r^*,t,r_s)$ is given by the matrix element in (20), which can be evaluated directly as a sum over eigenfunctions $\psi_\alpha(\mathbf{r})$ and eigenvalues ϵ_α of the harmonic oscillator Hamiltonian

$$n_T^{(0)}(\mathbf{r},\mu_c,\beta_c) = \sum_\alpha |\psi_\alpha(\mathbf{r})|^2(e^{(\beta\epsilon_\alpha-\nu_0)}+1)^{-1}. \quad \text{(B8)}$$

The activity ν_0 is determined by the condition that the density integrate to $\overline{N}$. A simpler practical approximation is given by the Thomas-Fermi or local density approximation

$$n^{(0)}(\mathbf{r},\mu_c,\beta_c) \simeq \frac{2}{h^3}\int d\mathbf{p}\left\{e^{-\nu_0}e^{\beta[\frac{p^2}{2m}+v(r)]}+1\right\}^{-1} = \lambda^{-3}\frac{4}{\sqrt{\pi}}I_{\frac{1}{2}}[\nu_0-\beta v(\mathbf{r})], \quad \text{(B9)}$$

where $v(r)$ is the harmonic trap potential, and the Fermi function $I_\alpha(\nu_0)$ and thermal de Broglie wavelength λ are defined by

$$I_\alpha(\nu_0) = \int_0^\infty dx\frac{x^\alpha}{e^{x-\nu_0}+1}, \quad \lambda = \left(\frac{2\pi\hbar^2\beta}{m}\right)^{1/2}. \quad \text{(B10)}$$

The validity of this Thomas-Fermi approximation for the conditions considered here is demonstrated in Appendix C.

With this choice for the reference density (B6) and (B7) become

$$n(\mathbf{r},\mu_c,\beta_c) = N\frac{n^{(0)}(\mathbf{r})e^{\Delta U(\mathbf{r},\mu_c,\beta_c|n)}}{\int d\mathbf{r}' n^{(0)}(\mathbf{r}')e^{\Delta U(\mathbf{r}',\mu_c,\beta_c|n)}}, \quad \text{(B11)}$$

$$\Delta U(\mathbf{r},\mu_c,\beta_c \mid n) = \int d\mathbf{r}'[c(|\mathbf{r}-\mathbf{r}'|,\mu_c,\beta_c)n(\mathbf{r}',\mu_c,\beta_c) - c^{(0)}(|\mathbf{r}-\mathbf{r}'|,\mu_c,\beta_c)n^{(0)}(\mathbf{r}',\mu_c,\beta_c)], \quad \text{(B12)}$$

where $c_T(r,\mu_c,\beta_c) \to c^{(0)}(r,\mu_c,\beta_c)$ corresponding to the noninteracting limit. Clearly, $n(\mathbf{r},\mu_c,\beta_c) \to n^{(0)}(\mathbf{r},\mu_c,\beta_c)$ in the absence of Coulomb interactions. Although it is not needed for calculation of (B11), the effective trap potential is determined

from

$$\beta_c[\mu_{ec} - v_c(\mathbf{r})]^{(0)} = \ln\left[n^{(0)}(\mathbf{r})\lambda_c^3\right] + \int \times d\mathbf{r}' c^{(0)}(|\mathbf{r}-\mathbf{r}'|,\mu_c,\beta_c) n^{(0)}(\mathbf{r}',\mu_c,\beta_c). \tag{B13}$$

This is used in the calculations for Fig. 3(b).

It is instructive to look at the limit of zero temperature. A Sommerfeld expansion of the local density (B9) gives

$$n^{*(0)}(\mathbf{r}^*,t=0,r_s) = \begin{cases} 0.034 r_s^{3/2}\left(\frac{2\nu_0}{\Gamma} - r^{*2}\right)^{3/2}, & r^* < \sqrt{\frac{2\nu_0}{\Gamma}}, \\ 0, & r^* \geqslant \sqrt{\frac{2\nu_0}{\Gamma}}, \end{cases} \tag{B14}$$

where $t\nu_0$ is determined from normalization

$$\nu_0 = 0.783 \overline{N}^{1/3} \frac{r_s^{1/2}}{t}, \quad \frac{2\nu_0}{\Gamma} = 2.88 \frac{\overline{N}^{1/3}}{r_s^{1/2}}. \tag{B15}$$

The density is concave from the origin until $r^* = \sqrt{2.88 \frac{\overline{N}^{1/3}}{r_s^{1/2}}}$, beyond which it vanishes. This vanishing of the density implies that the associated effective classical confining potential develops a hard wall. For the case of Fig. 4, $\overline{N} = 100, r_s = 18.4$, this gives $r^* \simeq 1.77$. The shell structure of Figs. 2 and 4 are finite temperature precursors of this limit.

With $n^{*(0)}(\mathbf{r}^*,t=0,r_s)$ known, the effective confining potential can be determined from (B12), where the exact Fourier transform of the ideal gas direct correlation function has the simple form [42]

$$\tilde{c}^{(0)}(k^*,t=0,r_s) = r_0^3\left(1 - \frac{1}{\frac{3}{4k_F^*}k^* - \frac{1}{16k_F^*}k^{*3}}\right). \tag{B16}$$

Here $k_F^* = k_F r_0 = (9\pi/4)^{1/3}$ and $k_F = (3\pi^2 n)^{1/3}$ is the Fermi wavelength.

2. Weak Coulomb limit

The noninteracting limit of the previous section has only exchange correlations among the particles to provide quantum effects on the effective trap. A better limit, incorporating some mean-field Coulomb interactions as well is given by the weak Coulomb coupling approximation in density functional theory (Hartree plus exchange). Within the same Thomas-Fermi approximation as (B9), this is

$$\begin{aligned} n_T(\mathbf{r},\mu_c,\beta_c) &\to n^{(w)}(\mathbf{r},\mu_c,\beta_c) \\ &\equiv \frac{2}{h^3}\int d\mathbf{p}\left(e^{-\nu_0} e^{\{\beta[\frac{p^2}{2m} + v(\mathbf{r})] + \beta v^{(w)}(\mathbf{r})\}} + 1\right)^{-1} \\ &= \lambda^{-3}\frac{4}{\sqrt{\pi}} I_{\frac{1}{2}}\{[\nu_0 - \beta v(\mathbf{r}) - \beta v^{(w)}(\mathbf{r})]\}. \end{aligned} \tag{B17}$$

The potential $v^{(w)}(\mathbf{r})$ representing the effects of Coulomb interactions among the particles is given by

$$v^{(w)}(\mathbf{r}) = q^2 \int d\mathbf{r}' \frac{n^{(w)}(\mathbf{r}')}{|\mathbf{r}-\mathbf{r}'|} + v_x[n^{(w)}(\mathbf{r})]. \tag{B18}$$

The first term is the mean-field Coulomb contribution (Hartree), while the second term $v_x[n(\mathbf{r})]$ is the local density approximation for exchange (density derivative of the exchange free energy [41]):

$$v_x[n(\mathbf{r})] = -\frac{e^2}{\sqrt{\pi}\lambda} I_{-\frac{1}{2}}[\nu_0(\mathbf{r})]. \tag{B19}$$

The density dependence of $v_x(n)$ is determined by inverting the ideal gas relationship

$$n(\mathbf{r}) = \lambda^{-3}\frac{4}{\sqrt{\pi}} I_{\frac{1}{2}}[\nu_0(\mathbf{r})]. \tag{B20}$$

It remains to determine the corresponding approximation to the classical direct correlation function, $c_T \to c^{(w)}$. Since (B18) results from an expansion of the Kohn-Sham potential to leading order in the Coulomb coupling constant Γ, the function $c^{(w)}$ is the corresponding weak-coupling (small Γ) limit of c,

$$c^{(w)}(|\mathbf{r}-\mathbf{r}'|,\mu_c,\beta_c) = c^{(0)}(|\mathbf{r}-\mathbf{r}'|,\mu_c,\beta_c) + \Gamma c^{(1)}(|\mathbf{r}-\mathbf{r}'|,\mu_c,\beta_c), \tag{B21}$$

and accordingly $\Delta U(\mathbf{r},\mu_c,\beta_c \mid n)$ in (B12) becomes

$$\begin{aligned} \Delta U(\mathbf{r},\mu_c,\beta_c \mid n) \to \int d\mathbf{r}' \{ &[c(|\mathbf{r}-\mathbf{r}'|,\mu_c,\beta_c) n(\mathbf{r}',\mu_c,\beta_c)] \\ &- [c^{(0)}(|\mathbf{r}-\mathbf{r}'|,\mu_c,\beta_c) \\ &+ \Gamma c^{(1)}(|\mathbf{r}-\mathbf{r}'|,\mu_c,\beta_c)] \\ &\times n^{(w)}(\mathbf{r}',\mu_c,\beta_c)\}. \end{aligned} \tag{B22}$$

The analytic calculation of $c^{(1)}$ from expansion in Γ does not lead to a simple, practical result. Instead, it can be calculated numerically from the HNC equations using a small value for Γ and writing

$$c^{(1)}(r,\mu_c,\beta_c) = \lim \frac{1}{\Gamma}[c(r,\mu_c,\beta_c) - c^{(0)}(r,\mu_c,\beta_c)]. \tag{B23}$$

In terms of the variables t, r_s the notion of small Γ is ambiguous:

$$\Gamma = \frac{\beta q^2}{r_0} = \frac{r_s}{t}\frac{2}{\left(\frac{9}{4}\pi\right)^{2/3}}. \tag{B24}$$

However, since the noninteracting case depends only on t the charge coupling can be considered the effect which introduces the r_s dependence. Hence, Γ should be made small by choosing the appropriate values for $r_s \ll 1$. Then $c^{(1)}$ will be a function of t alone.

In summary, with the limit density $n^{(w)}(\mathbf{r},\mu_c,\beta_c)$ and $\Delta U(\mathbf{r},\mu_c,\beta_c \mid n)$ given by (B22) the dimensionless forms (31) and (32) of the text are obtained. If desired, the effective trap can be calculated from (B4), which becomes

$$\begin{aligned} &[\beta\mu_{ec} - \beta v_c(\mathbf{r},\mu_c,\beta_c)]^{(w)} \\ &= \ln\left[n^{(w)}(\mathbf{r},\mu_c,\beta_c)\lambda_c^3\right] \\ &\quad - \int d\mathbf{r}'[c^{(0)}(|\mathbf{r}-\mathbf{r}'|,\mu_c,\beta_c) \\ &\quad + \Gamma c^{(1)}(|\mathbf{r}-\mathbf{r}'|,\mu_c,\beta_c)] n^{(w)}(\mathbf{r}',\mu_c,\beta_c). \end{aligned} \tag{B25}$$

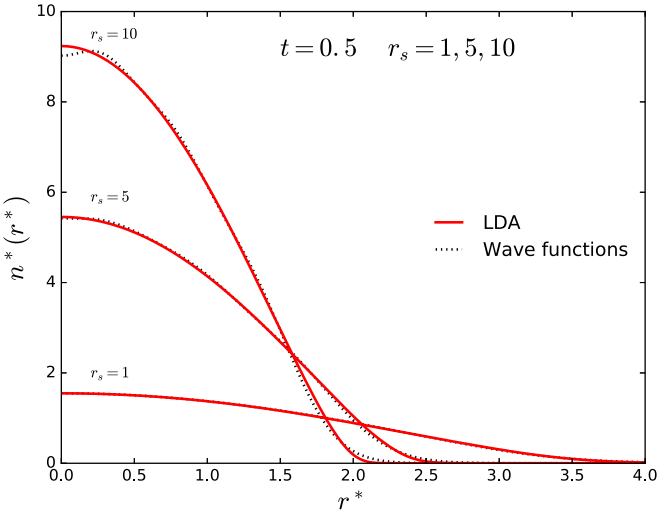

FIG. 8. Comparison of density profiles calculated with Harmonic oscillator wave functions (black dotted lines) and with the Thomas-Fermi approximation (red solid lines) for $t = 0.5$ and $r_s = 1,5,10$.

APPENDIX C: VALIDITY OF THOMAS-FERMI FORMS

Consider again (B8) for the noninteracting density

$$n^{*(0)}(r,t,r_s) = r_0^{*3} \sum_\alpha |\psi_\alpha(\mathbf{r})|^2 (e^{\beta(\epsilon_\alpha - \mu_c)} + 1)^{-1} \qquad \text{(C1)}$$

and its Thomas-Fermi (local density) approximation (B9)

$$n^{*(0)}(r,t,r_s) \simeq \left(\frac{r_0^*}{\lambda}\right)^3 \frac{4}{\sqrt{\pi}} I_{\frac{1}{2}}\left[\left(\beta\mu_e - \frac{1}{2}\Gamma r^{*2}\right)\right]. \qquad \text{(C2)}$$

Both are normalized to $\overline{N} = 100$. Figure 8 shows their comparison at $t = 0.5$ for $r_s = 1,5,10$. The agreement is quite good even for these low temperatures. Normally one would expect the Thomas-Fermi form to be applicable only at temperatures well above the Fermi temperature and for smooth densities. Evidently, the large particle number considered here has extended its validity to lower temperatures.

[1] *Frontiers and Challenges in Warm Dense Matter*, edited by F. Graziani *et al.* (Springer, Heidelberg, 2014); R. P. Drake, Phys. Today **63**, 28 (2010), and references therein.
[2] F. Perrot and M. W. C. Dharma-wardana, Phys. Rev. B **62**, 16536 (2000).
[3] J. W. Dufty and S. Dutta, Contrib. Plasma Phys. **52**, 100 (2012); Phys. Rev. E **87**, 032101 (2013).
[4] S. Dutta and J. Dufty, Phys. Rev. E **87**, 032102 (2013).
[5] S. Dutta and J. Dufty, Euro. Phys. Lett. **102**, 67005 (2013).
[6] Y. Liu and J. Wu, J. Chem. Phys. **140**, 084103 (2014).
[7] E. W. Brown, B. K. Clark, J. L. DuBois, and D. M. Ceperley, Phys. Rev. Lett. **110**, 146405 (2013).
[8] T. Pohl, T. Pattard, and J. M. Rost, Phys. Rev. Lett. **92**, 155003 (2004).
[9] O. Arp, D. Block, A. Piel, and A. Melzer, Phys. Rev. Lett. **93**, 165004 (2004); O. Arp, D. Block, M. Bonitz, H. Fehske, V. Golubnychiy, S. Kosse, P. Ludwig, A. Melzer, and A. Piel, J. Phys. Conf. Series **11**, 234 (2005).
[10] P. Ludwig, S. Kosse, and M. Bonitz, Phys. Rev. E **71**, 046403 (2005).
[11] M. Bonitz, D. Block, O. Arp, V. Golubnychiy, H. Baumgartner, P. Ludwig, A. Piel, and A. Filinov, Phys. Rev. Lett. **96**, 075001 (2006).
[12] V. Golubnychiy, H. Baumgartner, M. Bonitz, A. Filinov, and H. Fehske, J. Phys. A **39**, 4527 (2006).
[13] H. Baumgartner, H. Kählert, V. Golubnychiy, C. Henning, S. Käding, A. Melzer, and M. Bonitz, Contrib. Plasma Phys. **47**, 281 (2007); H. Baumgartner, D. Asmus, V. Golubnychiy, P. Ludwig, H. Kählert, and M. Bonitz, New J. Phys. **10**, 093019 (2008).
[14] W. D. Kraeft and M. Bonitz, J. Phys. Conf. Ser. **35**, 94 (2006).
[15] J. Cioslowski and E. Grzebielucha, Phys. Rev. E **78**, 026416 (2008).
[16] J. Wrighton, J. W. Dufty, H. Kählert, and M. Bonitz, Phys. Rev. E **80**, 066405 (2009).
[17] J. Wrighton, J. W. Dufty, M. Bonitz, and H. Kählert, Contrib. Plasma Phys. **50**, 26 (2010).
[18] W. G. van der Wiel, S. De Franceschi, J. M. Elzerman, T. Fujisawa, S. Tarucha, and L. P. Kouwenhoven, Rev. Mod. Phys. **75**, 1 (2002).
[19] S. M. Reimann and M. Manninen, Rev. Mod. Phys. **74**, 1283 (2002).
[20] H. Haug and S. W. Koch, in *Quantum Theory of the Optical and Electrical Properies of Semiconductors*, 4th ed. (World Scientific, London, 2004)
[21] L. P. Kouwenhoven, D. G. Austing, and S. Tarucha, Rep. Prog. Phys. **64**, 701 (2001); R. Hanson, L. P. Kouwenhoven, J. R. Petta, S. Tarucha, and L. M. K. Vandersypen, Rev. Mod. Phys. **79**, 1217 (2007).
[22] I. Bloch, Nat. Phys. **1**, 23 (2005).
[23] S. Giorgini, L. P. Pitaevksii, and S. Stringari, Rev. Mod. Phys. **80**, 1215 (2008).
[24] J. Lutsko, in *Advances in Chemical Physics*, edited by S. Rice (J. Wiley, Hoboken, NJ, 2010), Vol. 144.
[25] J.-P. Hansen and I. MacDonald, *Theory of Simple Liquids*, (Academic Press, London, 2006).
[26] M. Allen and D. Tildesley, *Computer Simulation of Liquids* (Oxford University Press, New York, 1989).
[27] F. Perrot and M. W. C. Dharma-wardana, Phys. Rev. Lett. **87**, 206404 (2001).
[28] M. W. C. Dharma-wardana and F. Perrot, Phys. Rev. Lett. **90**, 136601 (2003).
[29] M. W. C. Dharma-wardana, Phys. Rev. B **72**, 125339 (2005).
[30] M. W. C. Dharma-wardana, Int. J. Quantum Chem. **112**, 53 (2012).
[31] M. W. C. Dharma-wardana, Contrib. Plasma Phys. **55**, 85 (2015).
[32] M. W. C. Dharma-wardana, Computation **4**, 16 (2016).

[33] J. Wrighton, J. W. Dufty, and S. Dutta, in *Advances in Quantum Chemistry* (Elsevier, New York, 2015), Vol. 71.
[34] M. Bonitz, C. Henning, and D. Block, Rep. Prog. Phys. **73**, 066501 (2010).
[35] A. Melzer and D. Block in *Introduction to Complex Plasmas*, edited by M. Bonitz, H. Horing, and P. Ludwig (Springer-Verlag, New York, 2010).
[36] M. Bonitz, P. Ludwig, H. Baumgartner, C. Henning, A. Filinov, D. Block, O. Arp, A. Piel, S. Käding, Y. Ivanov, A. Melzer, H. Fehske, and V. Filinov, Phys. Plasmas **15**, 055704 (2008).
[37] P. Attard, J. Chem. Phys. **91**, 3072 (1989).
[38] J. Wrighton, H. Kählert, T. Ott, P. Ludwig, H. Thomsen, J. Dufty, and M. Bonitz, Contrib. Plasma Phys. **52**, 45 (2012).
[39] C. R. McDonald, G. Orlando, J. W. Abraham, D. Hochstuhl, M. Bonitz, and T. Brabec, Phys. Rev. Lett. **111**, 256801 (2013).
[40] J. W. Abraham and M. Bonitz, Contrib. Plasma Phys. **54**, 27 (2014).
[41] F. Perrot, Phys. Rev. A **20**, 586 (1979).
[42] C. Amovilli and N. H. March, Phys. Rev. B **76**, 195104 (2007).
[43] G. Kelbg, Ann. Phys. **467**, 219 (1963).
[44] A. V. Filinov, V. O. Golubnychiy, M. Bonitz, W. Ebeling, and J. W. Dufty, Phys. Rev. E **70**, 046411 (2004).